Molecular Cancer Therapeutics

Restricted Delivery of Talazoparib Across the Blood–Brain Barrier Limits the Sensitizing Effects of PARP Inhibition on Temozolomide Therapy in Glioblastoma

Sani H. Kizilbash[1], Shiv K. Gupta[2], Kenneth Chang[2], Ryo Kawashima[2], Karen E. Parrish[3], Brett L. Carlson[2], Katrina K. Bakken[2], Ann C. Mladek[2], Mark A. Schroeder[2], Paul A. Decker[4], Gaspar J. Kitange[2], Yuqiao Shen[5], Ying Feng[5], Andrew A. Protter[6], William F. Elmquist[3], and Jann N. Sarkaria[2]

Abstract

Poly ADP-ribose polymerase (PARP) inhibitors, including talazoparib, potentiate temozolomide efficacy in multiple tumor types; however, talazoparib-mediated sensitization has not been evaluated in orthotopic glioblastoma (GBM) models. This study evaluates talazoparib ± temozolomide in clinically relevant GBM models. Talazoparib at 1–3 nmol/L sensitized T98G, U251, and GBM12 cells to temozolomide, and enhanced DNA damage signaling and G_2–M arrest *in vitro*. *In vivo* cyclical therapy with talazoparib (0.15 mg/kg twice daily) combined with low-dose temozolomide (5 mg/kg daily) was well tolerated. This talazoparib/temozolomide regimen prolonged tumor stasis more than temozolomide alone in heterotopic GBM12 xenografts [median time to endpoint: 76 days versus 50 days temozolomide ($P = 0.005$), 11 days placebo ($P < 0.001$)]. However, talazoparib/temozolomide did not accentuate survival beyond that of temozolomide alone in corresponding orthotopic xenografts [median survival 37 vs. 30 days with temozolomide ($P = 0.93$), 14 days with placebo, $P < 0.001$]. Average brain and plasma talazoparib concentrations at 2 hours after a single dose (0.15 mg/kg) were 0.49 ± 0.07 ng/g and 25.5±4.1 ng/mL, respectively. The brain/plasma distribution of talazoparib in Bcrp$^{-/-}$ versus wild-type (WT) mice did not differ, whereas the brain/plasma ratio in Mdr1a/b$^{-/-}$ mice was higher than WT mice (0.23 vs. 0.02, $P < 0.001$). Consistent with the *in vivo* brain distribution, overexpression of MDR1 decreased talazoparib accumulation in MDCKII cells. These results indicate that talazoparib has significant MDR1 efflux liability that may restrict delivery across the blood–brain barrier, and this may explain the loss of talazoparib-mediated temozolomide sensitization in orthotopic versus heterotopic GBM xenografts. *Mol Cancer Ther; 16(12); 2735–46. ©2017 AACR.*

Downloaded from http://aacrjournals.org/mct/article-pdf/16/12/2735/1852933/2735.pdf by guest on 24 April 2025

Introduction

Temozolomide is an important component of therapy for patients with glioblastoma (GBM); however, emergence of drug resistance leads to inevitable disease recurrence and dismal prognosis despite optimal therapy (1, 2). Mechanisms of temozolomide resistance include the direct repair of temozolomide-induced O^6-methylguanine (O^6MeG) lesions by O^6-methylguanine-DNA-methyltransferase (MGMT; refs. 1, 3, 4) and N^7-methylguanine (N^7MeG) and N^3-methyladenine (N^3MeA) lesions by the base excision repair (BER; refs. 5, 6). Mutations in mismatch repair genes (7–9) and redundancies in DNA repair pathways also contribute toward temozolomide resistance (10). Thus, targeting DNA repair is expected to enhance the therapeutic efficacy of temozolomide (11). The PARP family of enzymes is responsible for the poly ADP-ribosylation (PARylation) of numerous DNA repair proteins; PARP1 also functions as a scaffold to recruit BER components XRCC1 and DNA polymerase-β to apurinic sites (11, 12). Therefore, PARP inhibition is thought to potentiate temozolomide efficacy by disrupting BER-mediated repair of the temozolomide-induced DNA lesions N^7MeG and N^3MeA (13), However, prior studies from our laboratory suggest that the presence of O^6MeG lesions may be necessary for PARP inhibitor–induced temozolomide sensitization *in vivo* (14–16). This capacity of PARP inhibitors to sensitize cancer cells to temozolomide has emerged as a promising strategy for patients with GBM.

Differences in molecular structure among PARP inhibitors greatly influence their biological effects beyond PARP inhibition alone (17). The trapping of PARP1/2 on chromatin by certain PARP inhibitors generates PARP–DNA complexes thought to be more

[1]Department of Oncology, Mayo Clinic, Rochester, Minnesota. [2]Department of Radiation Oncology, Mayo Clinic, Rochester, Minnesota. [3]Brain Barriers Research Center, University of Minnesota, Minneapolis, Minnesota. [4]Division of Biomedical Statistics and Informatics, Mayo Clinic, Rochester, Minnesota. [5]BioMarin Pharmaceutical Inc., Novato, California. [6]Medivation, San Francisco, California.

Note: Supplementary data for this article are available at Molecular Cancer Therapeutics Online (http://mct.aacrjournals.org/).

S.H. Kizilbash and S.K. Gupta contributed equally to this article.

Current address for A.A. Protter: Capella Bioscience, Inc. 550 Hamilton Ave, Palo Alto, CA 94301.

Corresponding Author: Jann N. Sarkaria, Mayo Clinic, 200 First Street SW; Rochester, MN 55905. Phone: 507-284-9025; Fax: 507-284-3906; E-mail: sarkaria.jann@mayo.edu

doi: 10.1158/1535-7163.MCT-17-0365

©2017 American Association for Cancer Research.

cytotoxic than unrepaired single-stand DNA breaks caused by inhibition of PARP enzymatic activity, and the trapping ability of various PARP inhibitors has been a crucial measure of their potency (17). The most potent PARP trapping agent, talazoparib, induces a 100-fold greater PARP trapping than olaparib and rucaparib, and is associated with increased cytotoxicity in BRCA-deficient tumor models (18–20). Moreover, talazoparib binds to the variable D-loop of PARP1/2, shorter D-loop in PARP3, and tankyrases cannot accommodate talazoparib, leading to decreased off-target effects (21). Furthermore, the significant efficacy of talazoparib when combined with low-dose temozolomide in multiple tumor models indicates that the cytotoxicity of the combination may be initiated by non-O^6MeG adducts (N^7MeG and N^3MeA) that promote PARP trapping (22). Although heterotopic GBM models were included in this evaluation, these models may not account for tissue specific constraints, including the role of the blood–brain barrier (BBB) associated with GBM therapy. Here, we investigated the efficacy of talazoparib/temozolomide in both GBM cell lines and patient-derived xenograft (PDX) models. After determining a tolerable *in vivo* talazoparib/temozolomide regimen, the efficacy was assessed in both heterotopic and orthotopic PDX GBM models. Finally, mechanisms that influence the distribution of talazoparib across the BBB were investigated.

Materials and Methods

Cell culture and drugs

Short-term explant cultures of the GBM12 PDX line were raised in neural stem cell media (Stem Pro NSC SFM; Invitrogen; ref. 15). U251 (MGMT-low) and T98G (MGMT-high) glioma cell lines obtained from the ATCC in the years 1998 and 2012, respectively, and were authenticated by short tandem repeat analysis (23, 24) performed by the ATCC in November 2013. Madin-Darby canine kidney II (MDCKII) cells overexpressing either human multidrug resistance protein 1 (MDR1) or murine breast cancer resistance protein (BCRP1) were gifts from Dr. Piet Borst in the year 1996 and Dr. Alfred Schinkel in the year 2003), respectively (Netherlands Cancer Institute, Amsterdam, the Netherlands). Cell lines were maintained in DMEM (VWR) supplemented with 10% FBS (Atlanta Biologicals) and 1% penicillin/streptomycin (Thermo Fisher Scientific). To ensure quality control, cell cultures were routinely tested for *Mycoplasma* at 6 months interval using MycoAlert *Mycoplasma* Detection Kit (catalog no. LT07-418, Lonza) as per the manufacturer's instruction manual. If necessary, cultures were treated with 50 μg/mL plasmocin (InVivogen). CyQuant, clonogenic, and neurosphere formation assays were performed as described previously (15).

Radiolabeled ^{3}H-vinblastine and ^{3}H-prazosin were procured from Moravek Biochemicals and PerkinElmer, respectively. For *in vitro* studies, temozolomide (Sigma-Aldrich), talazoparib (Medivation), zosuquidar (MDR1 inhibitor, Lilly; ref. 25), and Ko143 (BCRP inhibitor, Tocris; ref. 26) were dissolved in DMSO and stored at −20°C. For in vivo studies, temozolomide (Mayo Clinic Pharmacy) was suspended in Ora-plus (Perrigo) and talazoparib in 10% dimethylacetamide (Sigma-Aldrich)/5% Solutol HS15 (Sigma-Aldrich)/85% PBS. Both drugs were administered by oral gavage.

Western blotting and immunofluorescence

Dose response for PARP inhibition and analysis of talazoparib/temozolomide-induced DNA damage signaling were evaluated as described previously (15). Briefly, cells were treated with the indicated concentrations of talazoparib, temozolomide or their combination for 24–48 hours. Extracted proteins were analyzed by Western blotting using the antibodies phospho-S345-Chk1, phospho-T68-Chk2, β-actin, PARP1, Histone H3 (Cell Signaling Technology); Chk1, Chk2 (Millipore); phospho-S824-KAP1, PARP2 (Abcam); PAR (Trevigen), and KAP1 (Santa Cruz Biotechnology) as described in Supplementary Methods. Densitometry on original blots was quantified by ImageJ software and the signal was normalized to the corresponding control lane. Chromatin trapping of PARP1 and PARP2 was assessed by incubating U251 cells for 3 hours with graded concentrations of talazoparib in the presence of 100 μmol/L of temozolomide. Chromatin-bound proteins isolated by acid extraction were analyzed by Western blotting. To assess Ki67, glass slides carrying tissue sections were subjected to antigen retrieval in boiling Tris-sodium chloride buffer (pH 9.0) followed by immunostaining with Ki-67–specific rat mAb (eBioresource, catalog no. SolA15), and processed for immunofluorescence detection and analysis as described in Supplementary Methods. For detection of γH2AX and RPA foci, cells cultured on glass coverslips were treated with temozolomide and/or talazoparib for 24 or 72 hours and processed as described previously (15).

Flow cytometry

Cells treated with temozolomide and/or talazoparib were fixed in ice-cold 70% ethanol, incubated with RNase A and propidium iodide, and subsequently analyzed by flow cytometry as described previously (27). Modeling of cell-cycle events was performed using Modfit-LT version 4.

In vivo efficacy studies

All animal experiments were preapproved by the Institutional Animal Care and Use Committee (IACUC), and conducted in accordance with IACUC guidelines. Xenografts were established in female athymic nude mice (Hsd:athymic Nude-Foxn1^{nu}, ages 6–7 weeks; Envigo) as described previously (15, 16). Mice with established tumors were randomized into treatment groups. Treatment arms included placebo, a range of temozolomide-dosing schedules (5–50 mg/kg, days 1–5, repeated every 14 or 28 days), a range of talazoparib (0.025 or 0.15 mg/kg, days 1–5, repeated every 14 or 28 days), or a talazoparib/temozolomide combination. Heterotopic flank tumors were measured thrice weekly, and mice were euthanized when tumor volume exceeded 2,000 mm^3. Mice with intracranial xenografts were observed daily and euthanized upon reaching a moribund state.

Evaluation of pharmacodynamic effects

Pharmacodynamic effects were evaluated in mice with established flank tumors treated with vehicle, temozolomide (5 mg/kg/d), talazoparib (0.15 mg/kg, twice daily), or the combination of temozolomide and talazoparib for 5 days and then euthanized 72 hours after the last temozolomide dose. Tumors were harvested and processed for protein extraction and immunoblotting as described previously (15).

Central nervous system drug distribution

Nontumor-bearing FVB wild-type (WT), Mdr1a/b$^{-/-}$ (MKO), Bcrp$^{-/-}$ (BKO), and Mdr1a/b$^{-/-}$Bcrp$^{-/-}$ knockout (TKO) mice were treated with a single dose of talazoparib (0.15 mg/kg) and

Downloaded from http://aacrjournals.org/mct/article-pdf/16/12/2735/1852933/2735.pdf by guest on 24 April 2025

euthanized 2 hours after drug administration; whole blood and brain were collected for analysis. Plasma isolated by centrifugation and the brain tissues were flash frozen on dry ice and homogenized in three volumes of 5% BSA per plasma volume (or brain weight; talazoparib concentrations were determined by LC/MS-MS.

In vitro analyses of intracellular talazoparib accumulation

In vitro intracellular talazoparib accumulation was assessed by using vector-controlled MDCKII cells that overexpressed either human MDR1, or murine Bcrp1 as described previously (28). Cells were cultured to 80% confluence, rinsed with serum-free assay buffer, and pretreated with (or without) 1 μmol/L zosuquidar or 0.2 μmol/L Ko143 for 30 minutes, and subsequently supplemented with talazoparib, ^{3}H-vinblastine, or ^{3}H-prazosin. After incubation at 37°C for 1 hour, cells were rinsed with ice-cold PBS and lysed with 1% Triton X-100 (Thermo Fisher Scientific) and talazoparib concentrations determined by LC/MS-MS.

Analysis of talazoparib by LC/MS-MS

Talazoparib was extracted from cell lysate, brain homogenate, or plasma with cold ethyl acetate. The organic supernatant was dried with nitrogen, and the sample was reconstituted in 50 μL of 5 mmol/L ammonium acetate in acetonitrile (mobile phase). Five-microliter samples were injected onto the column (Agilent Zorbax SB C18 5 μm; 150 × 0.5 mm), and LC/MS-MS was performed on an LTQ Orbitrap Velos instrument (Thermo Fisher Scientific) interfaced with a Nano2D–LC HPLC (Eksigent) using positive electrospray ionization. Separation on the column was performed using a linear gradient (relative acetonitrile to 5 mmol/L ammonium acetate concentrations varied between 20% and 90%) at a mobile phase flow rate of 15 μL/minute. Analysis was performed using accurate mass extracted ion chromatograms of m/z 285.08997+ and 298.07922+ (parent ion m/z 381.1) for talazoparib with a mass tolerance of 2 ppm.

Statistical analyses

Unless stated otherwise, all in vitro data presented are mean ± SEM from three or more experiments. Two-sample *t* tests were used to compare measures across treatment groups. The IC_{50} values were calculated by fitting the experimental data to a sigmoidal curve using GraphPad Prism. Combination effects of talazoparib and temozolomide on cell growth were assessed by the Bliss independence log synergy volumes (μM^2%), which were calculated using MacSynergy II and reported in the form of three-dimensional graphs with temozolomide and talazoparib concentrations plotted on the X and Y dimensions, and Bliss independence log synergy volume on Z dimension (29). Median survival and tumor progression beyond 1,500 mm^3 (time to endpoint) were estimated by the Kaplan–Meier method and compared using the log-rank test. In all cases, P values <0.05 were considered statistically significant.

Results

Talazoparib sensitizes GBM cells to temozolomide

The inhibitory dose response of PARP activity by talazoparib was initially evaluated in U251 and T98G cell lines exposed to 100 μmol/L of hydrogen peroxide to maximally stimulate PARP activity. A near complete suppression of PARylation occurred at 3 nmol/L and 10 nmol/L of talazoparib in U251 and T98G cells, respectively (Fig. 1A). In the presence of 100 μmol/L of temozolomide, talazoparib also induced robust trapping of PARP1 and PARP2 at concentrations of 3 nmol/L and higher in U251 cells (Fig. 1B). These results affirm the potent PARP-inhibitory and trapping effects of talazoparib in GBM cells.

Higher concentrations of talazoparib (10 nmol/L in U251; 30 nmol/L in T98G cells) were needed for enhanced cytotoxicity as compared with controls (Fig. 1C and D). Although combining talazoparib with temozolomide significantly increased cytotoxicity in U251 cells (Fig. 1C; Supplementary Fig. S1A), cumulative synergy was minimal (12.4 μM^2%; Fig. 1C and E). In contrast, low concentrations of talazoparib (1–3 nmol/L) robustly enhanced temozolomide (3–100 μmol/L) cytotoxicity in T98G cells (Fig. 1D; Supplementary Fig. S1B) and demonstrated marked synergy (84.0 μM^2%; Fig. 1D and E). The increased sensitivity to talazoparib in the MGMT-expressing T98G cell line is predicted because of the lack of lethal O^6MeG. The presence of O^6MeG in temozolomide-treated U251 cells (MGMT nonexpressing) minimizes the impact of talazoparib-induced conversion of N^7 and N^3 adducts to cytotoxic lesions. Similar sensitizing effects of talazoparib were also observed in clonogenic assays with an additive effect of talazoparib combined with temozolomide (3.4 μM^2%) in U251 cells (Supplementary Fig. S2A and S2C), and a more significant synergy (34.3 μM^2%) with low-dose talazoparib combined with temozolomide in T98G cells (Supplementary Fig. S2B and S2C). These results suggest that talazoparib potentiates temozolomide efficacy in both temozolomide-sensitive and -resistant GBM cell lines.

Talazoparib potentiates DNA damage signaling and G_2–M cell-cycle arrest

Incubation with talazoparib (1–10 nmol/L) had no significant impact on the phosphorylation of Chk1, Chk2, or KAP1 in either of the glioma cell lines while exposure to clinically relevant temozolomide concentrations expectedly induced DNA damage signaling in U251 cells but not in T98G cells (Fig. 2A). However, cotreatment with talazoparib (3 or 10 nmol/L) and temozolomide (10 or 30 μmol/L) robustly increased phosphorylation of Chk1, Chk2, and KAP1 in U251 cells. Similarly, talazoparib (1–10 nmol/L) combined with supratherapeutic concentrations of temozolomide (300 μmol/L) increased the phosphorylation of all three DNA damage signaling proteins in T98G cells, while combining talazoparib (3 or 10 nmol/L) with 30 μmol/L temozolomide increased the phosphorylation of KAP1 and Chk2 but had no impact on phospho-Chk1 (Fig. 2A; Supplementary Fig. S3A). Similarly, talazoparib (3 nmol/L) had no effect on γH2AX or RPA foci compared with DMSO treatment in either U251 or T98G cells, while treatment with temozolomide (100 μmol/L) increased γH2AX and RPA foci in U251 (but not in T98G) cells. Cotreatment with talazoparib and temozolomide increased foci formation in both glioma cell lines (Fig. 2B–C). Cell-cycle analyses by flow cytometry demonstrated increased G_2–M arrest with talazoparib/temozolomide cotreatment as compared with treatment with either drug alone (Supplementary Fig. S4). These results suggested that talazoparib promotes temozolomide-induced DNA damage and signaling response in GBM cells.

Downloaded from http://aacrjournals.org/mct/article-pdf/16/12/2735/1852933/2735.pdf by guest on 24 April 2025

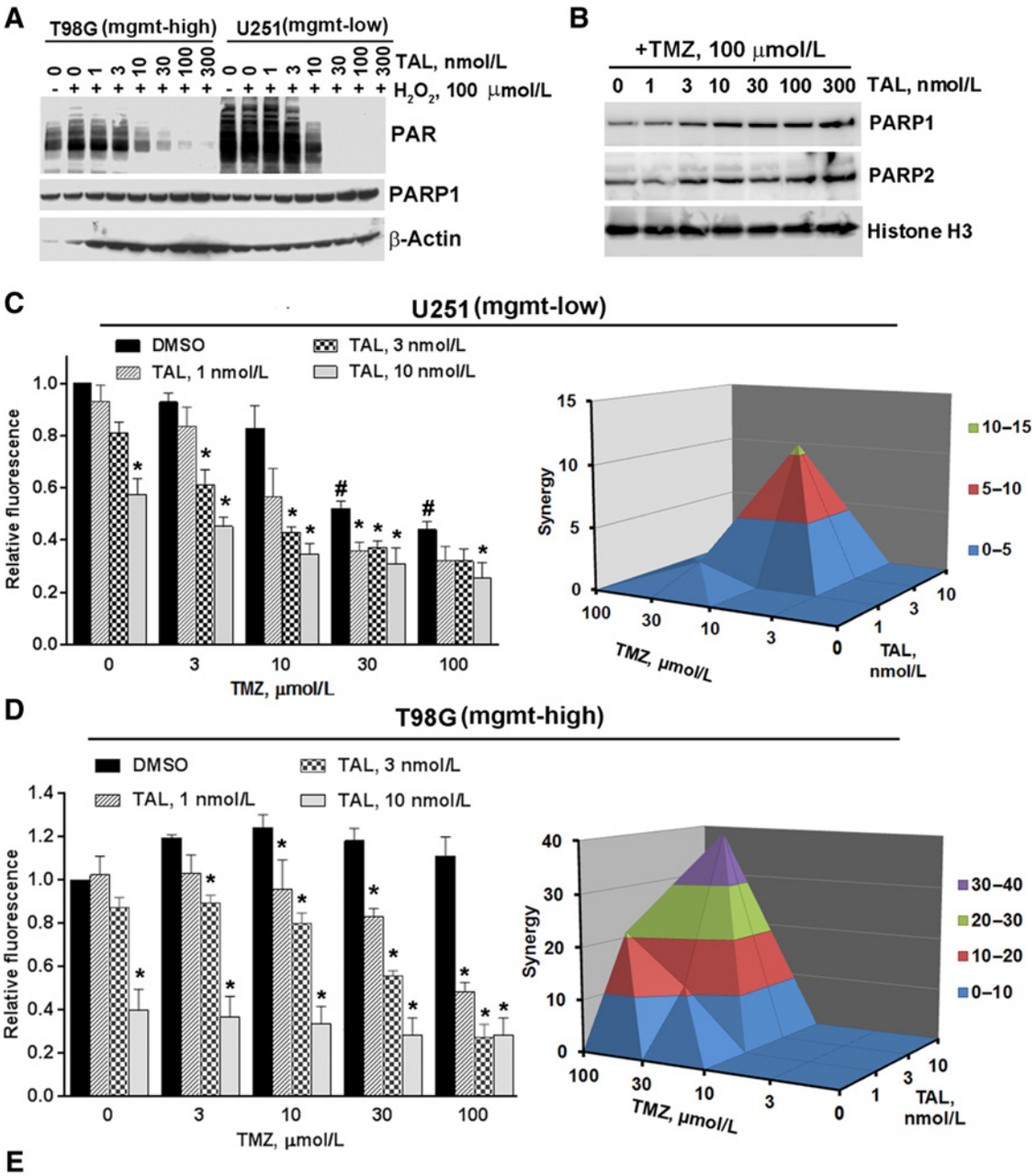

E

Cell line	Synergy volume at 95% CI (μM²%)	Antagonism volume at 95% CI (μM²%)	Combination effect
T98G	83.95	0	High synergy
U251	12.43	0	Limited synergy

Figure 1.

In vitro evaluation of sensitizing effects of talazoparib (TAL) in GBM cell lines. **A,** Western blot images showing dose-dependent inhibition of hydrogen peroxide (H_2O_2)–induced PARylation, total PARP1 and β-actin were used as loading controls. **B,** Western blots analysis of nuclear lysates to assess chromatin trapping of PARP1 and PARP2 in U251 cells after 3 hours of treatment with each of the talazoparib concentrations combined with 100 μmol/L of temozolomide (TMZ). **C** and **D,** Bar graphs (mean ± SEM from three independent experiments) showing effects of talazoparib ± temozolomide on cell growth assessed by CyQuant assay for U251 (**C**) or T98G (**D**) cells cultured for 5 days in the absence or presence of indicated concentrations of temozolomide ± talazoparib; *, $P < 0.05$ for with TAL treatments versus control; #, $P < 0.05$ for temozolomide treatment versus no temozolomide. The 3D plots shown on the right are synergy plots at 95% confidence interval (CI) for the data presented in bar graphs on left. **E,** Overall drug interaction measured as cumulative synergy or antagonism across the range of temozolomide and talazoparib concentrations.

Downloaded from http://aacrjournals.org/mct/article-pdf/16/12/2735/1852933/2735.pdf by guest on 24 April 2025

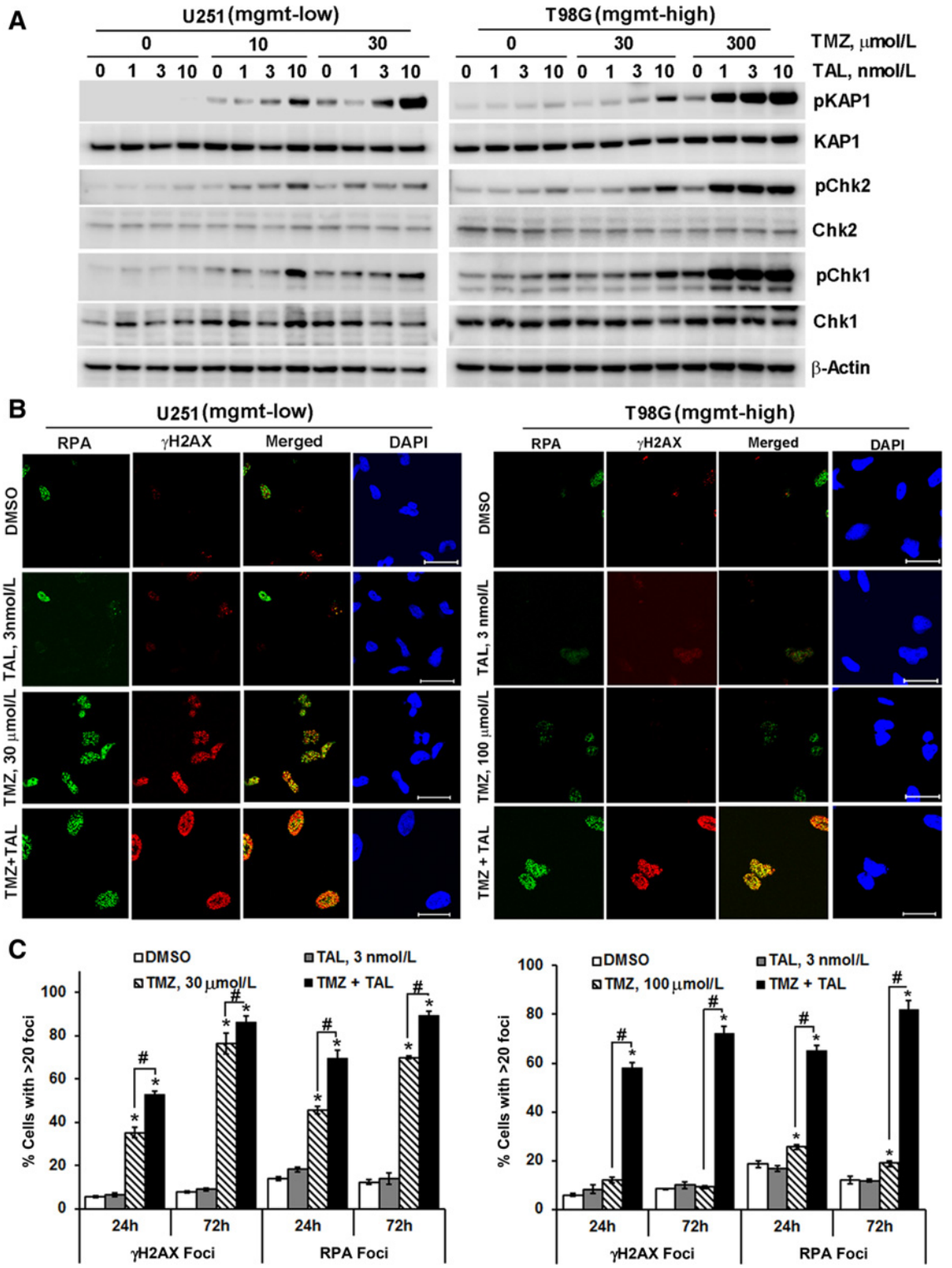

Figure 2.

Talazoparib (TAL)-mediated potentiation of temozolomide (TMZ)-induced DNA damage. **A,** Western blot images (representative from three independent experiments) showing the impact of a 24-hour pretreatment with talazoparib ± temozolomide on DNA damage signaling in U251 (MGMT-low) and T98G (MGMT-high) cells. **B,** Representative images of γH2AX (red) and RPA (green) foci in U251 and T98G cells treated with or without 3 nmol/L talazoparib and ± 100 μmol/L temozolomide; magnification bar, 50 μm. **C,** Quantification of cells with γH2AX or RPA staining (>20 foci/nuclei) from three independent experiments; *, $P < 0.05$ as compared with control; #, $P < 0.05$ for temozolomide versus talazoparib + temozolomide.

Downloaded from http://aacrjournals.org/mct/article-pdf/16/12/2735/1852933/2735.pdf by guest on 24 April 2025

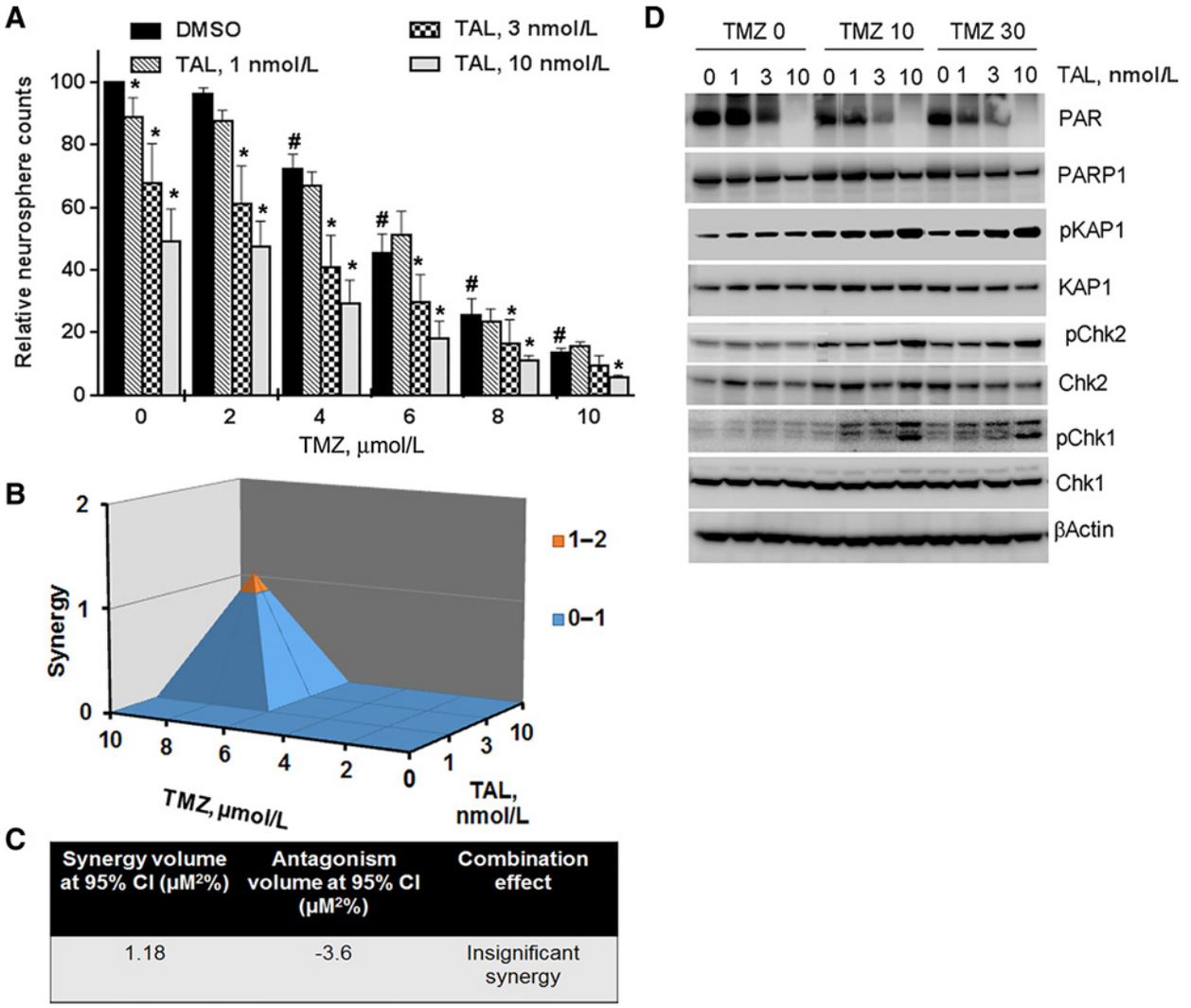

Figure 3.

In vitro evaluation of sensitizing effects of talazoparib (TAL) in GBM12 cells. **A,** Bar graphs (mean ± SEM from three independent experiments) showing effect of graded concentrations of talazoparib ± temozolomide (TMZ) on neurosphere formation; *, $P < 0.05$ for talazoparib versus DMSO; #, $P < 0.05$ for temozolomide versus control. **B,** The 3D plots showing synergy at 95% CI for the temozolomide/talazoparib combinations presented in **A**. **C,** Overall drug interaction presented as cumulative synergy and antagonism. **D,** Western blot images showing the impact of a 24-hour pretreatment with talazoparib ± temozolomide on DNA damage signaling in neurosphere cultures. β-Actin was used as a loading control.

Temozolomide-sensitizing effects of talazoparib on primary neurosphere growth *in vitro*

The *in vitro* efficacy of talazoparib was also assessed in the MGMT promoter hypermethylated GBM12 PDX line. GBM12 is sensitive to temozolomide alone with an IC_{50} of 5.1 μmol/L, and treatment with talazoparib (3 or 10 nmol/L) alone also led to reduced neurosphere formation (Fig. 3A; Supplementary Fig. S1C). Cotreatment of talazoparib with temozolomide led to a further 55%–70% reduction in neurosphere formation with a consequent reduction in temozolomide IC_{50} to 3.1 μmol/L and 81 nmol/L with talazoparib concentrations of 3 or 10 nmol/L, respectively. However, this drug interaction was not associated with any significant synergy (Fig. 3B and C). These results are similar to the limited synergy observed in U251 cells.

The effect of talazoparib, temozolomide, and the combination on DNA damage signaling was also examined in neurosphere cultures. Low-dose talazoparib (1 or 3 nmol/L) had a modest effect on PARP activity, as measured by the auto-PARylation of PARP1, whereas 10 nmol/L talazoparib effectively suppressed PARP activity (Fig. 3D; Supplementary Fig. S3B). Temozolomide (10 or 30 μmol/L) had no significant effect on PARP activity. talazoparib (1–10 nmol/L) alone had no significant impact on the phosphorylation of Chk1, Chk2, or KAP1 in GBM12. However, as compared with DMSO control or talazoparib (1–10 nmol/L) alone, treatment with temozolomide (10 or 30 μmol/L) led to increased KAP1 phosphorylation, and a modest but dose-dependent increase in phosphorylation of Chk1 and Chk2. The combination of talazoparib (10 nmol/L) and temozolomide (10

Downloaded from http://aacrjournals.org/mct/article-pdf/16/12/2735/1852933/2735.pdf by guest on 24 April 2025

Table 1. Evaluation of tolerability of treatment regimens combining talazoparib and temozolomide in nude mice implanted with GBM12 cells

#	Tumor location	Dose and schedule	Survival after 1 week of first dose	Survival after 4 weeks of first dose	Maximum weight loss
1	Orthotopic	TMZ: 50 mg/kg, d1–5, q28d + TAL: 0.025 mg/kg, bid, d1–5, q28d	0/5	0/5	23%
2	Orthotopic	TMZ: 30 mg/kg, d1–5, q28d + TAL: 0.05 mg/kg, bid, d1–5, q28d	0/5	0/5	24%
3	Orthotopic	TMZ: 5 mg/kg, d1–5, q28d + TAL: 0.05 mg/kg, bid, d1–5, q28d	5/5	4/5	1%
4	Orthotopic	TMZ: 5 mg/kg, d1–5, q28d + TAL: 0.075 mg/kg, bid, d1–5, q28d	5/5	3/5	6%
5	Flank	TMZ: 5 mg/kg, d1–5, q7d + TAL: 0.15 mg/kg, bid, d1–5, q7d	7/7	4/7	16%
6	Flank	TMZ: 5 mg/kg, d1–5, q14d + TAL: 0.15 mg/kg, bid, d1–5, q14d	11/11	10/11	7%

Abbreviations: bid, twice daily; TAL, talazoparib; TMZ, temozolomide.

or 30 μmol/L) robustly increased phosphorylation of all three DNA damage signaling proteins (Fig. 3D). The effect of combining lower dose talazoparib (1 or 3 nmol/L) with temozolomide on DNA damage signaling was modest and resulted in a minor increase in pKAP1, and no significant change in pChk1 or pChk2. These results are consistent with the idea that inhibition of PARP activity is necessary to potentiate the effect of temozolomide on DNA damage signaling in neurosphere cultures of GBM12. These *in vitro* analyses suggest that the combination of talazoparib and temozolomide may be an effective strategy to suppress GBM growth.

In vivo tolerability of talazoparib/temozolomide in mice

In vivo studies in athymic nude mice were initially performed to define a tolerable combination dosing regimen. Low-dose talazoparib (0.025 mg/kg twice daily) combined with standard temozolomide (50 mg/kg/d) on days 1–5 of a 28-day cycle led to substantial weight loss (23%) and 100% mortality within one week (Table 1). Combining talazoparib 0.15 mg/kg twice daily with a metronomic temozolomide regimen (5 mg/kg/d, days 1–5 every 7 days) was better tolerated with a median weight loss of 16% and a 42% mortality rate within 28 days. Reducing the dosing frequency (days 1–5 every 14 days) further improved tolerability (7% weight loss and 9% mortality in the first 28 days); therefore, this regimen was selected for further *in vivo* studies.

In vivo survival studies in PDX GBM12 treated with talazoparib/temozolomide

The efficacy of talazoparib and temozolomide was initially evaluated in flank GBM12 tumor models to avoid the potential confounding influence of drug delivery across the BBB. Talazoparib (0.15 mg/kg, twice daily, days 1–5 every 14 days) was inefficacious (11 vs. 14 days with control, $P = 0.19$) while temozolomide (5 mg/kg, days 1–5, every 14 days) significantly prolonged the time to tumor growth endpoint (50 vs. 11 days with placebo, $P < 0.001$; Fig. 4A; Supplementary Fig. S5). Cotreatment with talazoparib and temozolomide further extended the time to tumor growth endpoint (76 days vs. 50 days with temozolomide alone, $P = 0.005$; and 76 days vs. 11 days with placebo, $P < 0.001$; Fig. 4A). Terminal tumors acquired from animals treated with temozolomide or talazoparib/temozolomide showed no difference in Ki-67 staining compared to those treated with placebo or talazoparib alone (Supplementary Fig. S6). To assess pharmacodynamic effects of the treatment, mice with established flank GBM12 tumors were treated for 5 days and tumors were harvested 72 hours after treatment completion to analyze DNA damage signaling. Treatment with talazoparib had no effect on the phosphorylation of signaling proteins compared with control, while phosphorylation of KAP1, Chk1, and Chk2 signaling proteins clearly increased with temozolomide (Fig. 4B and C). The combination of talazoparib with temozolomide significantly increased pKAP1 and marginally increased pChk2, but did not influence Chk1 phosphorylation (Fig. 4B and C). These results indicate that talazoparib/temozolomide cotreatment is an effective strategy in heterotopic GBM12 xenografts.

The efficacy of talazoparib/temozolomide regimen was then tested in an orthotopic GBM12 tumor model. Talazoparib (0.15 mg/kg, twice daily, days 1–5, every 14 days) was inefficacious (14 vs. 14 days with placebo, $P = 0.46$), whereas temozolomide (5 mg/kg, days 1–5, every 14 days) doubled the median survival (30 days vs. 14 days with placebo, $P < 0.001$, Fig. 4D). Notably, this survival benefit with low-dose temozolomide was inferior to the survival extension previously reported for a more standard temozolomide regimen (50 mg/kg, days 1–5, every 28 days) in orthotopic GBM12 models (59 days; ref. 16). In contrast to the flank study, talazoparib/temozolomide cotreatment did not significantly increase median survival compared with temozolomide alone (37 days vs. 30 days with temozolomide alone, $P = 0.93$; 37 days vs. 14 days with placebo, $P < 0.001$, Fig. 4D). These results indicate that temozolomide was effective in both heterotopic and orthotopic GBM12 PDX tumors despite dose reduction, but the combination of temozolomide with talazoparib was only effective in heterotopic tumors.

Talazoparib brain/plasma distribution and efflux liability

The lack of talazoparib efficacy in the orthotopic tumor model may be explained by limitations in drug delivery across the BBB. Brain and plasma concentrations of talazoparib at two hours after a single dose (0.15 mg/kg) were 0.49 ± 0.07 ng/g (1.3 nmol/L) and 25.5 ± 4.1 ng/ml (67.1 nmol/L), respectively (brain-to-plasma ratio, 0.02). Efflux activity of MDR1 and/or BCRP1 is known to influence the delivery of numerous chemotherapeutic drugs across the BBB, so the brain-to-plasma ratio of talazoparib was additionally assessed in MKO, BKO, and TKO FVB mice. Talazoparib concentrations in the brain of BKO mice was no different than that of WT mice, while the concentrations of talazoparib were significantly higher in brain tissues of MKO and TKO mice, (17.2 ± 2.1 and 17.3 ± 3.8 ng/g; brain-to-plasma ratio 0.23 and 0.24, respectively; Fig. 5A). These results suggest that MDR1-mediated efflux at the BBB may significantly contribute to the limited distribution of talazoparib in the brain.

The efflux liability for talazoparib was further examined by assessing *in* vitro intracellular talazoparib accumulation in MDCKII cells modified to overexpress either human MDR1 or murine Bcrp1. Similar to the limited uptake of ^{3}H-vinblastine (a

Downloaded from http://aacrjournals.org/mct/article-pdf/16/12/2735/1852933/2735.pdf by guest on 24 April 2025

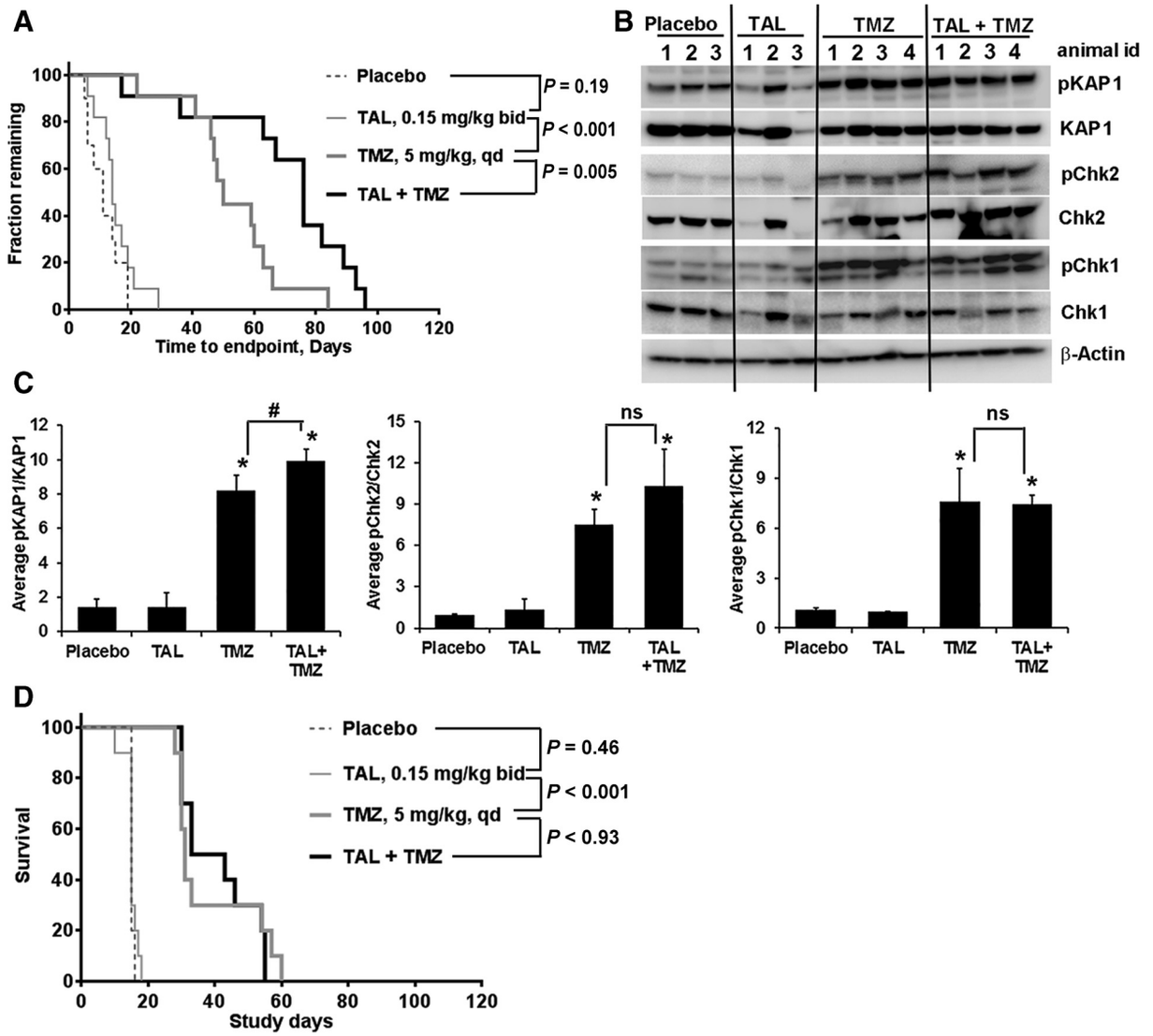

Figure 4.

Evaluation of *in vivo* sensitizing effects of talazoparib (TAL). **A,** Kaplan–Meier graphs showing time to end point (tumor volume 1,500 mm^3) in flank xenografts of GBM12 after cyclical treatment with placebo, talazoparib, temozolomide (TMZ), or talazoparib/temozolomide. **B,** Western blots of pharmacodynamic analysis performed in GBM12 flank xenografts treated as in **A** for 1 week, and euthanized 72 hours after the last dose of temozolomide, equal protein from 3 to 4 tumors per group were analyzed for phosphorylated and total KAP1, Chk2, and Chk1. β-Actin was used as a loading control. **C,** Bar graphs showing densitometric quantification of damage signaling from Western blots depicted in Fig. 2B. *, $P < 0.05$ for placebo versus treatment; #, $P < 0.05$ for TMZ versus TAL + TMZ. **D**, Kaplan–Meier graphs showing survival over time in mice with established orthotopic GBM12 xenografts treated as in **A**.

known MDR1 substrate), talazoparib accumulation was restricted in MDCKII-MDR1 cells to 18.6% ± 1.2% of the talazoparib concentrations in control cells ($P < 0.001$, Fig. 5B). Furthermore, the impact of MDR1 on talazoparib accumulation was completely reversed in the presence of 1 μmol/L zosuquidar (Fig. 5B). MDR1 inhibition also led to a smaller increase in talazoparib accumulation in control cells, which is consistent with known basal expression of MDR1 in MDCKII-WT cells. Talazoparib accumulation in MDCKII-BCRP1 cells was not altered (83.1% ± 4.4% as compared with control cells, $P = 0.06$; Fig. 5C), and inhibition of BCRP by 200 nmol/L Ko143 slightly increased talazoparib accumulation in MDCKII-BCRP cells but remained statistically insignificant relative to control cells (242% ± 46.9% vs. 99.1% ± 15.5%, $P = 0.13$). These results confirm a selective efflux liability of talazoparib toward MDR1.

Discussion

Combination therapy with PARP inhibitors and temozolomide is a promising strategy and is currently being clinically evaluated in several malignancies including breast cancer (NCT01506609, NCT01009788), small-cell lung cancer (NCT02152982, NCT01390571), and GBM (NCT02152982, NCT01390571). The potency of talazoparib at nanomolar concentrations

Downloaded from http://aacrjournals.org/mct/article-pdf/16/12/2735/1852933/2735.pdf by guest on 24 April 2025

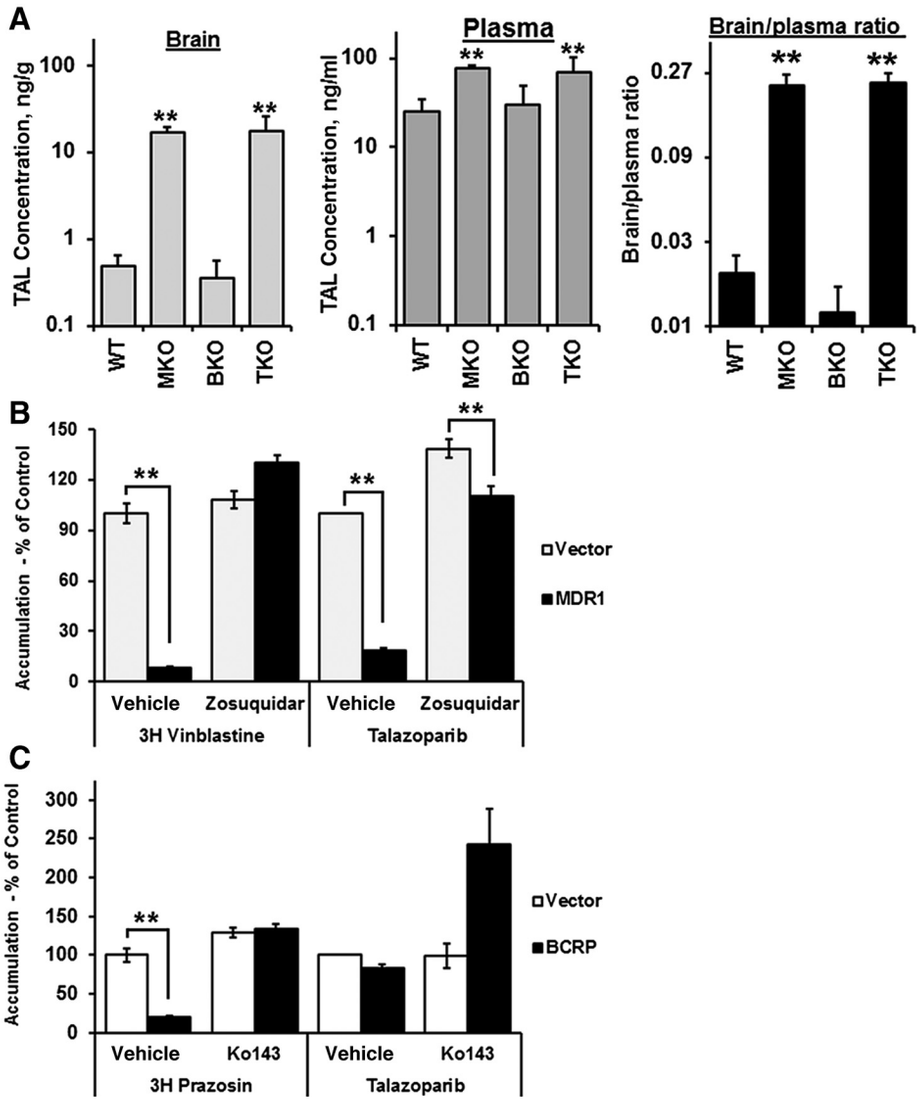

Figure 5.

Talazoparib (TAL) distribution in plasma and brain tissues. **A,** Bar graphs (mean ± SD) for TAL concentration in brain and plasma of FVB wild-type (WT), Mdr1a/b$^{-/-}$ (MKO), Bcrp1$^{-/-}$ (BKO), Mdr1a/b$^{-/-}$Bcrp1$^{-/-}$ triple knockout (TKO) mice at 2 hours after a single dose of talazoparib (0.15 mg/kg), ($n = 3$; **, $P < 0.05$ vs. WT controls). **B,** Bar graphs showing intracellular accumulations of talazoparib or vinblastine in vector control versus MDR1-overexpressing MDCKII cells treated with vinblastine (9.3 nmol/L) or talazoparib (1 μmol/L) ± 1 μmol/L zosuquidar, an MDR1 inhibitor. **C,** Bar graphs showing intracellular levels of prazosin or TAL in vector or BCRP1-overexpressing MDCKII cells treated with prazosin (0.39 nmol/L) or talazoparib (1 μmol/L) ± BCRP1 inhibitor Ko143 (0.2 μmol/L), results are mean ± SD, $n = 3$; **, $P < 0.05$ compared with vector controls.

(18) and the specific synergy with temozolomide (18, 30) has generated interest for this combination. After showing promise in heterotopic xenografts of GBM and Ewing sarcoma (22), talazoparib/temozolomide has demonstrated preliminary efficacy in a phase I clinical trial in multiple tumor types (31). However efficacy in heterotopic GBM xenografts does not necessarily translate into orthotopic efficacy (32), so further investigation was critical prior to GBM clinical trial development. This study demonstrates a lack of efficacy of talazoparib/temozolomide in orthotopic GBM models in association with limited brain distribution of talazoparib, therefore suggesting that talazoparib/temozolomide may not be appropriate for clinical translation in GBM.

The mechanism of temozolomide sensitization by PARP inhibitors at clinically achievable concentrations remains unclear (15). PARP1 and 2 have a pleiotropic role in DNA repair, including the processing of temozolomide-induced N^3MeA and N^7MeG DNA lesions (11, 33). PARP inhibitors are thought to potentiate temozolomide by suppressing the BER-mediated repair of N^3MeA and N^7MeG DNA lesions. In addition, PARP trapping initiates cytotoxicity by generating protein–DNA complexes at BER intermediates, a mechanism that is distinct from the O^6MeG-mediated cytotoxicity of temozolomide alone (22). Supporting this notion, talazoparib (like veliparib) synergized the *in vitro* cytotoxic effects of temozolomide to a greater extent in temozolomide-resistant GBM cells (Fig. 1C). However, temozolomide resistance prevents *in vivo* sensitization by veliparib (14–16) suggesting that PARP inhibitor concentrations achievable *in vivo* may have little impact on BER. PARP additionally regulates MRN to promote the restart of stalled replication forks (34). Temozolomide-induced O^6MeG lesions mispair with thymidine in cells lacking MGMT, triggering futile cycles of mismatch repair, stalled replication, and double stranded DNA breaks (3). Thus, PARP inhibition and trapping may potentiate temozolomide efficacy by compromising fork stability and/or delayed recovery from replication stress. This paradigm is supported by the increased DNA damage signaling observed after *in vivo* treatment of MGMT promoter hypermethylated GBM xenografts with veliparib/temozolomide compared

Downloaded from http://aacrjournals.org/mct/article-pdf/16/12/2735/1852933/2735.pdf by guest on 24 April 2025

with temozolomide alone (16). The effect of talazoparib combined with low-dose temozolomide in the *in vivo* setting may be below the threshold required to induce a detectable impact on fork stability, despite a delayed recovery from replication stress as demonstrated by the prolongation of tumor stasis in heterotopic tumor xenografts (Fig. 4A–C). A dose-dependent influence on recovery from replication stress may be an alternative mechanism for talazoparib-mediated potentiation of temozolomide efficacy.

Dose reductions of temozolomide are necessary to promote the tolerability of some PARP inhibitors. In clinical trials of temozolomide combined with veliparib and rucaparib, 25%–30% dose reductions were essential to prevent significant myelotoxicity (35, 36). In contrast, the addition of talazoparib to temozolomide required an 80% reduction in temozolomide dose. This higher toxicity of talazoparib/temozolomide may be related to superior PARP trapping by talazoparib. Mouse xenograft studies have revealed an inverse correlation between PARP trapping capacity and the tolerability of PARP inhibitors when combined with temozolomide (20). Although there is clinical precedent for the use of lower doses of temozolomide per day for the treatment of GBM (RTOG 0525, RESCUE), the evaluated temozolomide doses (50–75 mg/m^2) exceeded the anticipated dose reduction for talazoparib/temozolomide tolerance, and these regimens were designed to deplete MGMT by increasing the overall treatment dose density (37, 38). With the scarcity of efficacy data for low-dose temozolomide in patients with newly diagnosed GBM, significant dose reductions of the only chemotherapy agent with known survival benefit to permit tolerability of a novel experimental agent with unknown clinical value may not be feasible. On the basis of synergy analysis in GBM cell lines, low-dose temozolomide regimens are more amenable for initial study in patients with recurrent malignancy (NCT02116777). However, talazoparib/temozolomide synergy in temozolomide-resistant models (T98G) was only possible at clinically unachievable temozolomide concentrations, rather than the lower doses needed for tolerability. These potential issues would need to be addressed before attempting further development of talazoparib/temozolomide in patients with GBM.

Drug exclusion from the brain by the BBB is a critical variable that limits the efficacy of many CNS-directed pharmaceutical agents. The BBB is a complex neurovascular unit that includes tight junctions between brain capillary endothelial cells and ATP-binding cassette transporters expressed on their luminal surfaces. The historical narrative has been that drug exposure in high-grade gliomas should be adequate because the contrast enhancement on MRI should correlate with BBB disruption. However infiltrating glioma cells extend well beyond the margins of contrast enhancement (39, 40). In addition, blood–glioma barrier breakdown is regional and heterogenous (28). The concentration of many drugs is significantly lower at the infiltrating GBM rim as compared with the necrotic tumor core (28). This impaired drug delivery to infiltrating glioma may be associated with diminished efficacy of these drugs in orthotopic glioma models (32, 41–43). Talazoparib mirrors these experiences by demonstrating a lack of orthotopic efficacy despite activity in heterotopic models. Furthermore, the concentration of talazoparib in the mouse brain (0.5 ng/g or 1.3 nmol/L) was lower than required for effective PARP inhibition *in vitro*, hence explaining the observed lack of intracranial efficacy. Moreover, this concentration increased 35-fold (17.2 ng/g) in MKO, providing clear evidence of the prominent liability of talazoparib to MDR1-mediated efflux at the BBB. These findings reinforce our hypothesis that the BBB restricts talazoparib delivery into the brain and prevents sufficient drug delivery for efficacy in brain tumors.

The repeated failures of numerous promising drugs in clinical trials for patients with GBM testifies for the necessity of careful preclinical evaluation of critical clinically relevant parameters prior to human study. The *in vivo* talazoparib dosing strategy and CNS distribution evaluation in this study were pertinent because the plasma concentration of talazoparib achieved two hours after drug administration was similar to that measured in the phase I clinical trial (67.1 nmol/L in mice vs. 50 nmol/L in human; ref. 44). Comparing the pharmacokinetics of talazoparib to other PARP inhibitors, the brain-to-plasma concentration ratio for talazoparib (0.02) is lower than that of rucaparib (0.11), which also lacked efficacy in orthotopic glioma models (42). Alternatively, veliparib has a much higher brain-to-plasma concentration ratio (0.47) than either talazoparib or rucaparib despite the efflux liability of veliparib to MDR1 and BCRP (16, 45). Furthermore, veliparib has clear efficacy in temozolomide-sensitive orthotopic glioma models despite being significantly less potent than talazoparib (inhibition of hydrogen peroxide induced PARylation at 1,000 nmol/L vs. 3 nmol/L with talazoparib; ref. 16). On the basis of these data, the phase II/III clinical trial A071102 was launched to evaluate the impact of veliparib added to standard adjuvant temozolomide therapy in patients with newly diagnosed, MGMT promoter hypermethylated GBM (tolerable doses of temozolomide/veliparib lack synergy in temozolomide-refractory GBM, as demonstrated in preclinical models (14, 16) and RTOG-0929 clinical trial (46)). A comparison of the properties of drugs from a single class provides insight on the relative significance of variables such as drug potency, BBB penetrability, and efflux liability for efficacy in orthotopic glioma models. These considerations emphasize the necessity to give special attention to brain pharmacokinetics and drug tolerability at clinically relevant concentrations for the successful design of GBM-directed novel therapeutics.

Disclosure of Potential Conflicts of Interest

No potential conflicts of interest were disclosed.

Authors' Contributions

Conception and design: S.H. Kizilbash, S.K. Gupta, K.E. Parrish, Y. Shen, A.A. Protter, W.F. Elmquist, J.N. Sarkaria

Development of methodology: S.H. Kizilbash, S.K. Gupta, K.E. Parrish, Y. Feng, W.F. Elmquist

Acquisition of data (provided animals, acquired and managed patients, provided facilities, etc.): S.H. Kizilbash, S.K. Gupta, K. Chang, R. Kawashima, B.L. Carlson, K.K. Bakken, A.C. Mladek, M.A. Schroeder, G.J. Kitange, W.F. Elmquist

Analysis and interpretation of data (e.g., statistical analysis, biostatistics, computational analysis): S.H. Kizilbash, S.K. Gupta, K. Chang, K.E. Parrish, A.C. Mladek, P.A. Decker, J.N. Sarkaria

Writing, review, and/or revision of the manuscript: S.H. Kizilbash, S.K. Gupta, K.E. Parrish, P.A. Decker, G.J. Kitange, Y. Shen, W.F. Elmquist, J.N. Sarkaria

Administrative, technical, or material support (i.e., reporting or organizing data, constructing databases): B.L. Carlson

Study supervision: S.K. Gupta, B.L. Carlson, J.N. Sarkaria

Other (provided compound and method of usage and relevant information on animal dosing etc.): Y. Feng

Acknowledgments

We thank Ms. Xiaoyue Chen, PhD student at Mayo Graduate School for advice on Ki-76 immunofluorescence, Mayo Optical Morphology and Flow Cytometry Core for help with flow cytometry; Analytical Biochemistry Core,

Downloaded from http://aacrjournals.org/mct/article-pdf/16/12/2735/1852933/2735.pdf by guest on 24 April 2025

University of Minnesota Masonic Cancer Center for help with LC-MS, and BioMarin Pharmaceuticals Inc. for supply of talazoparib.

The study was supported by the NIH grants R03 CA201612 (to S.K. Gupta), R01 CA176830 (to J.N. Sarkaria), RO1 CA138437 (to W.F. Elmquist), R01 NS77921 (to W.F. Elmquist and J.N. Sarkaria), and P50 CA108961. S.K. Gupta is partly supported through Eagles Cancer Funds, Mayo Clinic Cancer Center.

The costs of publication of this article were defrayed in part by the payment of page charges. This article must therefore be hereby marked *advertisement* in accordance with 18 U.S.C. Section 1734 solely to indicate this fact.

Received April 25, 2017; revised August 25, 2017; accepted September 11, 2017; published OnlineFirst September 25, 2017.

References

1. Hegi ME, Diserens AC, Gorlia T, Hamou MF, de Tribolet N, Weller M, et al. MGMT gene silencing and benefit from temozolomide in glioblastoma. N Engl J Med 2005;352:997–1003.
2. Friedman HS, Kerby T, Calvert H. Temozolomide and treatment of malignant glioma. Clin Cancer Res 2000;6:2585–97.
3. Sarkaria JN, Kitange GJ, James CD, Plummer R, Calvert H, Weller M, et al. Mechanisms of chemoresistance to alkylating agents in malignant glioma. Clin Cancer Res 2008;14:2900–8.
4. Kitange GJ, Carlson BL, Mladek AC, Decker PA, Schroeder MA, Wu W, et al. Evaluation of MGMT promoter methylation status and correlation with temozolomide response in orthotopic glioblastoma xenograft model. J Neurooncol 2009;92:23–31.
5. Agnihotri S, Gajadhar AS, Ternamian C, Gorlia T, Diefes KL, Mischel PS, et al. Alkylpurine-DNA-N-glycosylase confers resistance to temozolomide in xenograft models of glioblastoma multiforme and is associated with poor survival in patients. J Clin Invest 2012;122:253–66.
6. Agnihotri S, Burrell K, Buczkowicz P, Remke M, Golbourn B, Chornenkyy Y, et al. ATM regulates 3-methylpurine-DNA glycosylase and promotes therapeutic resistance to alkylating agents. Cancer Discov 2014;4:1198–213.
7. Cahill DP, Levine KK, Betensky RA, Codd PJ, Romany CA, Reavie LB, et al. Loss of the mismatch repair protein MSH6 in human glioblastomas is associated with tumor progression during temozolomide treatment. Clin Cancer Res 2007;13:2038–45.
8. Yip S, Miao J, Cahill DP, Iafrate AJ, Aldape K, Nutt CL, et al. MSH6 mutations arise in glioblastomas during temozolomide therapy and mediate temozolomide resistance. Clin Cancer Res 2009;15:4622–9.
9. Fortini P, Pascucci B, Parlanti E, D'Errico M, Simonelli V, Dogliotti E. The base excision repair: mechanisms and its relevance for cancer susceptibility. Biochimie 2003;85:1053–71.
10. Nagel ZD, Kitange GJ, Gupta SK, Joughin BA, Chaim IA, Mazzucato P, et al. DNA repair capacity in multiple pathways predicts chemoresistance in glioblastoma multiforme. Cancer Res 2017;77:198–206.
11. Helleday T, Petermann E, Lundin C, Hodgson B, Sharma RA. DNA repair pathways as targets for cancer therapy. Nat Rev Cancer 2008;8:193–204.
12. Liu X, Shi Y, Guan R, Donawho C, Luo Y, Palma J, et al. Potentiation of temozolomide cytotoxicity by poly(ADP)ribose polymerase inhibitor ABT-888 requires a conversion of single-stranded DNA damages to double-stranded DNA breaks. Mol Cancer Res 2008;6:1621–9.
13. Calabrese CR, Almassy R, Barton S, Batey MA, Calvert AH, Canan-Koch S, et al. Anticancer chemosensitization and radiosensitization by the novel poly(ADP-ribose) polymerase-1 inhibitor AG14361. J Natl Cancer Inst 2004;96:56–67.
14. Clarke MJ, Mulligan EA, Grogan PT, Mladek AC, Carlson BL, Schroeder MA, et al. Effective sensitization of temozolomide by ABT-888 is lost with development of temozolomide resistance in glioblastoma xenograft lines. Mol Cancer Ther 2009;8:407–14.
15. Gupta SK, Mladek AC, Carlson BL, Boakye-Agyeman F, Bakken KK, Kizilbash SH, et al. Discordant *in vitro* and *in vivo* chemopotentiating effects of the PARP inhibitor veliparib in temozolomide-sensitive versus -resistant glioblastoma multiforme xenografts. Clin Cancer Res 2014;20:3730–41.
16. Gupta SK, Kizilbash SH, Carlson BL, Mladek AC, Boakye-Agyeman F, Bakken KK, et al. Delineation of MGMT hypermethylation as a biomarker for veliparib-mediated temozolomide-sensitizing therapy of glioblastoma. J Natl Cancer Inst 2016;108:pii:djv369.
17. Murai J, Huang SY, Das BB, Renaud A, Zhang Y, Doroshow JH, et al. Trapping of PARP1 and PARP2 by clinical PARP inhibitors. Cancer Res 2012;72:5588–99.
18. Shen Y, Rehman FL, Feng Y, Boshuizen J, Bajrami I, Elliott R, et al. BMN 673, a novel and highly potent PARP1/2 inhibitor for the treatment of human cancers with DNA repair deficiency. Clin Cancer Res 2013;19:5003–15.
19. Murai J, Huang SY, Renaud A, Zhang Y, Ji J, Takeda S, et al. Stereospecific PARP trapping by BMN 673 and comparison with olaparib and rucaparib. Mol Cancer Ther 2014;13:433–43.
20. Hopkins TA, Shi Y, Rodriguez LE, Solomon LR, Donawho CK, DiGiammarino EL, et al. Mechanistic dissection of PARP1 trapping and the impact on in vivo tolerability and efficacy of PARP inhibitors. Mol Cancer Res 2015;13:1465–77.
21. Aoyagi-Scharber M, Gardberg AS, Yip BK, Wang B, Shen Y, Fitzpatrick PA. Structural basis for the inhibition of poly(ADP-ribose) polymerases 1 and 2 by BMN 673, a potent inhibitor derived from dihydropyridophthalazinone. Acta Crystallogr F Struct Biol Commun 2014;70:1143–9.
22. Smith MA, Reynolds CP, Kang MH, Kolb EA, Gorlick R, Carol H, et al. Synergistic activity of PARP inhibition by talazoparib (BMN 673) with temozolomide in pediatric cancer models in the pediatric preclinical testing program. Clin Cancer Res 2015;21:819–32.
23. Capes-Davis A, Reid YA, Kline MC, Storts DR, Strauss E, Dirks WG, et al. Match criteria for human cell line authentication: where do we draw the line? Int J Cancer 2013;132:2510–9.
24. Masters JR, Thomson JA, Daly-Burns B, Reid YA, Dirks WG, Packer P, et al. Short tandem repeat profiling provides an international reference standard for human cell lines. Proc Natl Acad Sci U S A 2001;98:8012–7.
25. Starling JJ, Shepard RL, Cao J, Law KL, Norman BH, Kroin JS, et al. Pharmacological characterization of LY335979: a potent cyclopropyldibenzosuberane modulator of P-glycoprotein. Adv Enzyme Regul 1997;37:335–47.
26. Allen JD, van Loevezijn A, Lakhai JM, van der Valk M, van Tellingen O, Reid G, et al. Potent and specific inhibition of the breast cancer resistance protein multidrug transporter in vitro and in mouse intestine by a novel analogue of fumitremorgin C. Mol Cancer Ther 2002;1:417–25.
27. Sarkaria JN, Tibbetts RS, Busby EC, Kennedy AP, Hill DE, Abraham RT. Inhibition of phosphoinositide 3-kinase related kinases by the radiosensitizing agent wortmannin. Cancer Res 1998;58:4375–82.
28. Agarwal S, Mittapalli RK, Zellmer DM, Gallardo JL, Donelson R, Seiler C, et al. Active efflux of Dasatinib from the brain limits efficacy against murine glioblastoma: broad implications for the clinical use of molecularly targeted agents. Mol Cancer Ther 2012;11:2183–92.
29. Prichard MN, Shipman C Jr.A three-dimensional model to analyze drug-drug interactions. Antiviral Res 1990;14:181–205.
30. Engert F, Schneider C, Weibeta LM, Probst M, Fulda S. PARP inhibitors sensitize Ewing sarcoma cells to temozolomide-induced apoptosis via the mitochondrial pathway. Mol Cancer Ther 2015;14:2818–30.
31. Wainberg ZA, Hecht JR, Konecny GE, Goldman JW, Sadeghi S, Chmielowski B, et al. Safety and efficacy results from a phase I dose -escalation trial of the PARP inhibitor talazoparib in combination with either temozolomide or irinotecan in patients with advanced malignancies. Cancer Res 2016;76(14 Suppl.): abstract CT011.
32. Pokorny JL, Calligaris D, Gupta SK, Iyekegbe DO Jr., Mueller D, Bakken KK, et al. The efficacy of the wee1 inhibitor MK-1775 combined with temozolomide is limited by heterogeneous distribution across the blood-brain barrier in glioblastoma. Clin Cancer Res 2015;21:1916–24.
33. Helleday T. The underlying mechanism for the PARP and BRCA synthetic lethality: clearing up the misunderstandings. Mol Oncol 2011;5:387–93.
34. Bryant HE, Petermann E, Schultz N, Jemth AS, Loseva O, Issaeva N, et al. PARP is activated at stalled forks to mediate Mre11-dependent replication restart and recombination. Embo J 2009;28:2601–15.
35. Plummer R, Lorigan P, Steven N, Scott L, Middleton MR, Wilson RH, et al. A phase II study of the potent PARP inhibitor, rucaparib (PF-01367338, AG014699), with temozolomide in patients with metastatic melanoma demonstrating evidence of chemopotentiation. Cancer Chemother Pharmacol 2013;71:1191–9.

Downloaded from http://aacrjournals.org/mct/article-pdf/16/12/2735/1852933/2735.pdf by guest on 24 April 2025

36. Su JM, Thompson P, Adesina A, Li XN, Kilburn L, Onar-Thomas A, et al. A phase I trial of veliparib (ABT-888) and temozolomide in children with recurrent CNS tumors: a pediatric brain tumor consortium report. Neuro Oncol 2014;16:1661–8.
37. Perry JR, Belanger K, Mason WP, Fulton D, Kavan P, Easaw J, et al. Phase II trial of continuous dose-intense temozolomide in recurrent malignant glioma: RESCUE study. J Clin Oncol 2010;28:2051–7.
38. Gilbert MR, Wang M, Aldape KD, Stupp R, Hegi ME, Jaeckle KA, et al. Dose-dense temozolomide for newly diagnosed glioblastoma: a randomized phase III clinical trial. J Clin Oncol 2013;31:4085–91.
39. Earnest Ft, Kelly PJ, Scheithauer BW, Kall BA, Cascino TL, Ehman RL, et al. Cerebral astrocytomas: histopathologic correlation of MR and CT contrast enhancement with stereotactic biopsy. Radiology 1988;166: 823–7.
40. Pafundi DH, Laack NN, Youland RS, Parney IF, Lowe VJ, Giannini C, et al. Biopsy validation of 18F-DOPA PET and biodistribution in gliomas for neurosurgical planning and radiotherapy target delineation: results of a prospective pilot study. Neuro Oncol 2013;15:1058–67.
41. Becker CM, Oberoi RK, McFarren SJ, Muldoon DM, Pafundi DH, Pokorny JL, et al. Decreased affinity for efflux transporters increases brain penetrance and molecular targeting of a PI3K/mTOR inhibitor in a mouse model of glioblastoma. Neuro Oncol 2015;17:1210–9.
42. Parrish KE, Cen L, Murray J, Calligaris D, Kizilbash S, Mittapalli RK, et al. Efficacy of PARP inhibitor rucaparib in orthotopic glioblastoma xenografts is limited by ineffective drug penetration into the central nervous system. Mol Cancer Ther 2015;14:2735–43.
43. Parrish KE, Pokorny J, Mittapalli RK, Bakken K, Sarkaria JN, Elmquist WF. Efflux transporters at the blood-brain barrier limit delivery and efficacy of cyclin-dependent kinase 4/6 inhibitor palbociclib (PD-0332991) in an orthotopic brain tumor model. J Pharmacol Exp Ther 2015;355:264–71.
44. De Bono JS, Mina LA, Gonzalez M, Curtin NJ, Wang E, Henshaw JW, et al. First-in-human trial of novel oral PARP inhibitor BMN 673 in patients with solid tumors. J Clin Oncol 2013;31(Suppl.): abstract: 2580.
45. Li X, Delzer J, Voorman R, de Morais SM, Lao Y. Disposition and drug-drug interaction potential of veliparib (ABT-888), a novel and potent inhibitor of poly(ADP-ribose) polymerase. Drug Metab Dispos 2011;39:1161–9.
46. Robins HI, Zhang P, Gilbert MR, Chakravarti A, de Groot JF, Grimm SA, et al. A randomized phase I/II study of ABT-888 in combination with temozolomide in recurrent temozolomide resistant glioblastoma: an NRG oncology RTOG group study. J Neurooncol 2016;126:309–16.

Downloaded from http://aacrjournals.org/mct/article-pdf/16/12/2735/1852933/2735.pdf by guest on 24 April 2025